Two $(\beta\alpha)_8$-Barrel Enzymes of Histidine and Tryptophan Biosynthesis Have Similar Reaction Mechanisms and Common Strategies for Protecting Their Labile Substrates[†,‡]

Martina Henn-Sax,[§,||] Ralf Thoma,[⊥,@] Steffen Schmidt,[||,#] Michael Hennig,[⊥,@] Kasper Kirschner,[⊥] and Reinhard Sterner*[,§,||]

Institut für Biochemie, Universität zu Köln, Otto-Fischer-Strasse 12-14, D-50674 Köln, Germany, Abteilung Molekulare Genetik und Präparative Molekularbiologie, Institut für Mikrobiologie und Genetik, Georg-August-Universität Göttingen, Grisebachstrasse 8, D-37077 Göttingen, Germany, Abteilung für Biophysikalische Chemie und Abteilung für Strukturbiologie, Biozentrum der Universität Basel, Klingelbergstrasse 70, CH-4056 Basel, Switzerland, Pharma Research 65/308, F. Hoffmann-La Roche AG, CH-4070 Basel, Switzerland, and European Molecular Biology Laboratory Heidelberg, Meyerhofstrasse 1, D-69117 Heidelberg, Germany

Received May 7, 2002; Revised Manuscript Received July 15, 2002

ABSTRACT: The enzymes *N*′-[(5′-phosphoribosyl)formimino]-5-aminoimidazole-4-carboxamide ribonucleotide isomerase (HisA) and phosphoribosylanthranilate isomerase (TrpF) are sugar isomerases that are involved in histidine and tryptophan biosynthesis, respectively. Both enzymes have the $(\beta\alpha)_8$-barrel fold and catalyze Amadori rearrangements of a thermolabile aminoaldose into the corresponding aminoketose. To identify those amino acids that are essential for catalysis, conserved residues at the active sites of both HisA and TrpF from the hyperthermophile *Thermotoga maritima* were replaced by site-directed mutagenesis, and the purified variants were investigated by steady-state enzyme kinetics. Aspartate 8, aspartate 127, and threonine 164 appeared to be important for the HisA reaction, whereas cysteine 7 and aspartate 126 appeared to be important for the TrpF reaction. On the basis of these results and the X-ray structure of a complex between TrpF and a bound product analogue, a reaction mechanism involving general acid−base catalysis and a Schiff base intermediate is proposed for both enzymes. A comparison of the HisA and TrpF enzymes from *T. maritima* and *Escherichia coli* showed that, at the physiological temperatures of 80 and 37 °C, respectively, the enzymes from the hyperthermophile have significantly higher catalytic efficiencies than the corresponding enzymes from mesophiles. These results suggest that HisA and TrpF have similar chemical reaction mechanisms and use the same strategy to prevent the loss of their thermolabile substrates.

Although contemporary enzymes are highly specific for their substrates, some of them show striking similarities with respect to their three-dimensional structures and reaction mechanisms, suggesting that they are evolutionarily related (*1*). The $(\beta\alpha)_8$-barrel is the most frequently encountered fold among enzymes and is adopted by ∼10% of all proteins with known structure (*2*, *3*). Comprehensive comparisons of amino acid sequences and reaction mechanisms, as well as protein engineering studies, support the idea that a large fraction of the known $(\beta\alpha)_8$-barrels has evolved from a common ancestral enzyme by divergent evolution (*4*−*6*).

N′-[(5′-Phosphoribosyl)formimino]-5-aminoimidazole-4-carboxamide ribonucleotide (ProFAR) isomerase (HisA)[1] and phosphoribosylanthranilate (PRA) isomerase (TrpF) are $(\beta\alpha)_8$-barrel enzymes of histidine and tryptophan biosynthesis, respectively, that catalyze similar Amadori rearrangements of aminoaldoses into the corresponding aminoketoses (Figure 1). Although the two enzymes share only an insignificant degree of sequence similarity of ∼10%, it was possible to establish TrpF activity on the scaffold of HisA from the hyperthermophile *Thermotoga maritima* (tHisA) by introducing a single amino acid exchange (*7*). This result

[†] This work was sponsored by grants from the Deutsche Forschungsgemeinschaft (Grant STE 891/4-1 to R.S.) and the Swiss National Science Foundation (Grant 31-45855 95 to K.K.). M.H.-S. was supported by a fellowship of the Hans-Böckler Foundation.

[‡] The coordinates of the complex between tTrpF and rCdRP have been deposited in the Protein Data Bank (entry 1LBM).

* To whom correspondence should be addressed. Phone: +49-221-470 6432. Fax: +49-221-470 6731. E-mail: Reinhard.Sterner@Uni-Koeln.de.

[§] Universität zu Köln.

[||] Georg-August-Universität Göttingen.

[⊥] Biozentrum der Universität Basel.

[@] F. Hoffmann-La Roche AG.

[#] European Molecular Biology Laboratory (EMBL) Heidelberg.

[1] Abbreviations: HisA, *N*′-[(5′-phosphoribosyl)formimino]-5-aminoimidazole-4-carboxamide ribonucleotide isomerase; ProFAR, *N*′-[(5′-phosphoribosyl)formimino]-5-aminoimidazole-4-carboxamide ribonucleotide; PRFAR, *N*′-[(5′-phosphoribulosyl)formimino]-5-aminoimidazole-4-carboxamide ribonucleotide; AICAR, 5-aminoimidazole-4-carboxamide ribotide; PRA, phosphoribosylanthranilate; CdRP, 1-[(2-carboxyphenyl)amino]-1-deoxyribulose 5-phosphate; rCdRP, reduced CdRP; ImGP, imidazole glycerol phosphate; TrpF, phosphoribosylanthranilate isomerase; tHisA, HisA from *T. maritima*; tTrpF, TrpF from *T. maritima*; eHisA, HisA from *E. coli*; eTrpF, TrpF from *E. coli*; tHisF, synthase subunit of the imidazole glycerol phosphate synthase from *T. maritima*; tHisH, glutaminase subunit of the imidazole glycerol phosphate synthase from *T. maritima*; sTrpC, indole-3-glycerol phosphate synthase from *Sulfolobus solfataricus*.

10.1021/bi026092h CCC: $22.00
Published on Web 09/14/2002

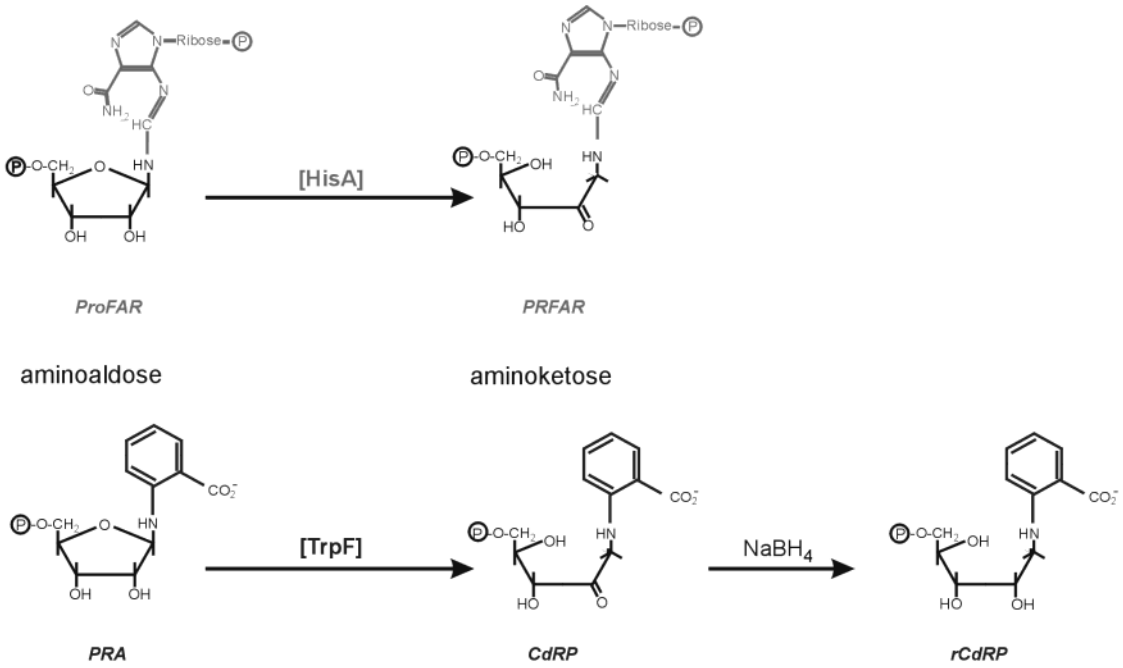

FIGURE 1: HisA and TrpF catalyze the Amadori rearrangements of aminoaldoses into aminoketoses during histidine and tryptophan biosynthesis. Reduction of CdRP, the product of the TrpF reaction, with sodium borohydride ($NaBH_4$) yields the stable product analogue rCdRP (*35*).

suggests that both enzymes evolved from an ancestral enzyme of broader substrate specificity, the reaction mechanism of which, however, has not yet been resolved.

A number of metabolites have short half-lives, especially at elevated temperatures (*8*). A chemically distinct subgroup of them are phosphoribosylamine derivatives such as phosphoribosylamine, the substrate of glycinamide ribonucleotide synthase participating in the de novo synthesis of purines (*9*), as well as PRA and ProFAR (*10*, *11*). The loss of a thermolabile metabolite can be avoided by at least two different mechanisms. One is the direct transfer of the metabolite from the producing to the consuming enzyme by "metabolic channeling" (*12*), which requires complex formation between the two enzymes. It was postulated to be responsible for the protection of phosphoribosylamine from hydrolysis (*9*). The other strategy is to convert the labile metabolite to a more stable product by its rapid turnover catalyzed by the enzyme downstream. For example, TrpF from *T. maritima* (tTrpF) processes PRA with a higher catalytic efficiency than TrpF from *Escherichia coli* (eTrpF), when compared at the physiological temperatures of 80 and 37 °C, respectively (*11*).

This work was undertaken to compare the reaction mechanisms of HisA and TrpF and the strategies by which these two enzymes protect their thermolabile substrates. It is shown that both Amadori rearrangements are supported by general acid−base catalysis of structurally conserved amino acids and that not only tTrpF but also tHisA protects its substrate with an unusually high catalytic efficiency at 80 °C. These results further support the assumed evolutionary relationship between these two enzymes from different metabolic pathways.

EXPERIMENTAL PROCEDURES

DNA Manipulation and Sequence Analysis. Preparation of DNA, amplification, extraction, digestion with restriction endonucleases, and sequencing were performed as described previously (*13*).

Expression of the E. coli hisA Gene and Purification of the Protein Product. The *his*A gene of *E. coli* (e*his*A) was amplified by PCR, using chromosomal DNA of strain DH5α as a template. The oligonucleotide 5′-GAGAT**CATATG**ATTATTCCGGCATTAGAT-3′ with an *Nde*I site (in bold) was used as the 5′-primer. The oligonucleotide 5′-GAGAC**GGATCC**TTATGCGTTTTGCCAGC-3′ with a *Bam*HI site (in bold) was used as the 3′-primer. Using the two introduced restriction sites, e*his*A was cloned into the expression plasmid pET 15b, yielding the plasmid pET 15b-e*his*A. In this system, the produced eHisA protein contains at the N-terminus a hexahistidine tag for Ni chelate affinity purification. Before expression, the insert was subjected to DNA sequencing to exclude inadvertent PCR mutations. Expression was conducted in *E. coli* BL21(DE3) cells, which contain the gene for the phage T7 polymerase on their chromosome. An overnight culture of freshly transformed cells containing 25 mL of LB medium supplemented with 0.15 mg/mL ampicillin was used to inoculate 2.5 L of the same medium. The culture was incubated at 30 °C with continuous stirring (100 rpm). For reasons unexplained so far, IPTG inhibits expression of e*his*A. Therefore, cells were grown overnight at 30 °C without addition of IPTG, resulting in an OD_{600} value of 4.5. Cells were centrifuged (Sorvall RC-3B, 4500 rpm, 35 min, 4 °C), washed with 50 mM potassium phosphate buffer at pH 7.5, and centrifuged again (Sorvall RC-5Cplus, SS34 rotor, 8000 rpm, 20 min, 4 °C). Approximately 14 g of cells (wet weight) was obtained, corresponding to 5.6 g/L of culture. It was reported that NaCl stabilizes the HisA enzyme of *Salmonella typhimurium* (*14*), the sequence of which is 93% identical with that of eHisA. Therefore, all purification steps were performed in the presence of 300−700 mM NaCl. The cells were resuspended (2 mL of buffer for 1 g of wet mass) in 50 mM potassium phosphate buffer (pH 7.5)

containing 0.3 mM phenylmethanesulfonyl fluoride and 3 μg/mL DNase and RNase and disrupted by sonification at 0 °C (Branson Sonifier 250, 2 × 2 min, 50% pulse, output control 5). The resulting homogenate was centrifuged (Sorvall RC-5Cplus, SS34 rotor, 15 000 rpm, 50 min, 4 °C), and NaCl and imidazole were added to final concentrations of 300 and 10 mM to the supernatant. The solution was centrifuged again under identical conditions. The clear supernatant was loaded on a Ni^{2+} chelate column (1.8 cm × 15 cm, Pharmacia) equilibrated with 50 mM potassium phosphate buffer (pH 7.5) containing 300 mM sodium chloride and 10 mM imidazole, at 4 °C. The column was washed with 8 volumes of equilibration buffer, and bound proteins were eluted with 300 mL of a linear gradient from 10 to 500 mM imidazole in equilibration buffer. The His-tagged eHisA eluted as a single peak, which however exhibited a broad shoulder. From here on, all buffer solutions contained 2 mM DTT to prevent aggregation of eHisA, which is probably due to the formation of unspecific intermolecular disulfide bonds. Fractions containing eHisA as judged by SDS−PAGE were pooled and dialyzed against 50 mM Tris-HCl buffer (pH 7.5) containing 700 mM NaCl and 2 mM DTT. Further purification was performed with high-speed perfusion chromatography using the $BioCAD_{Sprint}$ system (PerSeptive Biosystems, Inc.). To this end, the pooled and dialyzed eHisA was loaded on a Poros CHT10-I column (1.2 cm × 8.8 cm) containing hydroxyapatite that was equilibrated with 50 mM Tris-HCl buffer (pH 7.5) containing 300 mM NaCl and 2 mM DTT. The column was washed with 5 volumes of equilibration buffer, and bound proteins were eluted with 140 mL of a linear gradient from 0 to 100 mM sodium phosphate in equilibration buffer. eHisA eluted as two distinct peaks, a minor one at ~5 mM sodium phosphate and the main one at ~20 mM sodium phosphate. N-Terminal sequencing of the protein from the small peak showed that the residues methionine 1 and glycine 2 had been cleaved off. In contrast, in the protein from the main peak, only methionine 1 was missing. To investigate a homogeneous population of molecules, only fractions of the main peak were pooled, although eHisA from both peaks exhibited identical enzymatic activities. The pooled fractions were dialyzed against 50 mM potassium phosphate buffer (pH 7.5) containing 700 mM NaCl and 2 mM DTT, concentrated to 3 mg/mL by ultrafiltration (Centriprep 10, Amicon), and shock frozen in liquid nitrogen after addition of glycerol to a final concentration of 10%. eHisA was pure to more than 95%, as tested by both SDS−PAGE and reversed phase HPLC (data not shown). The purification yielded ~7 mg of eHisA per 14 g of wet cells. To remove the N-terminal His tag by proteolytic cleavage, 200 μL of eHisA [0.2 mg/mL in 50 mM Tris-HCl buffer (pH 8.5) containing 200 mM NaCl and 2 mM $CaCl_2$] was mixed with 5 μL of thrombin from human serum (Sigma, 100 units/mL) and incubated at 37 °C for 3 h. This treatment resulted in the removal of the His tag from only ~50% of the eHisA molecules, as judged by SDS−PAGE, and in a significant loss of enzymatic activity (data not shown).

Site-Directed Mutagenesis of thisA and ttrpF. Point mutations were introduced into the t*his*A and t*trp*F genes with the megaprimer method (*15*, *16*), using the plasmids pDS56/RBSII_t*his*A (*17*) and pET11c_t*trp*F (*18*) as templates. The following oligonucleotides were used for production of megaprimers (newly introduced restriction sites for the control of the reaction are in boldface type, and new codons to introduce an amino acid exchange are underlined). The 3′-primers 5′-CTG AAG AGA TTT ATC GCC GGG-3′ (*Bgl*II site deleted) for construction of t*his*A_D8N, 5′-GAG ATC CAC CAC GGC ATC AGT GTG AA-3′ (*Dra*III site deleted) for construction of t*his*A_H48A, 5′-CGC ATT CGA GAG AT**T** **CAC** **C**AC GTG AAT-3′ (new *Hph*I site) for construction of t*his*A_ D51N, and 5′-GTA ATC GAG CGA **ATT** **AAT** CCC GCC TCC-3′ (new *Vsp*I site) for construction of t*his*A_R83N were used together with the 5′-primer CyRI 5′-TCA CGA GGC CCT TTC GTC TT-3′. The 5′-primers 5′-GTA ATC GAG CG**A** **ATT** AAT CC CGC CTC C-3′ (new *Mse*I site) for construction of t*his*A_D127N and 5′-GAG ATC GT**A** **CAT** **GC**G GAG ATC-3′ (new *Nsp*I site) for construction of t*his*A_T164A were used together with the 3′-primer CyPstI 5′-TCG CCA GCT AGC TTG GAT TCT-3′. The 3′-primer 5′-CGT TAT **GCC** **GGC** GAT TTT CA-3′ (new *Nae*I site) was used together with the 5′-primer C7AU 5′-TGT GGC GCC GGT GAT GC-3′ for construction of t*trp*F_C7A, and the 5′-primer 5′-**GAA TTC** CCG ATT CTT CTC AAT ACG A-3′ (new *Eco*RI site) was used together with the 3′-primer T7E 5′-A TTA ATA CGA CTC ACT ATA GGG-3′ for construction of t*trp*F_D126N. The megaprimers were purified by agarose gel electrophoresis and used in the second PCR as 5′- or 3′-primers, together with CyPstI or CyRI for t*his*A, and T7E or C7AU for t*trp*F, to produce the full-length product. The double mutant t*trp*F_C7A_D126N was produced as described for t*trp*F_D126N, but pET11c-t*trp*F_C7A was used as a template. The full-length products were digested with *Pae*I and *Hin*dIII for t*his*A, and with *Nde*I and *Bam*HI for t*trp*F, and ligated into pDS56/RBSII and pET11c, respectively. To confirm the planned base substitutions and to exclude inadvertent point mutations, all t*his*A and t*trp*F gene variants were entirely sequenced.

Heterologous Expression of the thisA and ttrpF Gene Variants and Purification of the Protein Products. The t*his*A gene variants were heterologously expressed in *E. coli* and purified as described previously (*7*). The yields were between 2.8 and 4.3 mg of pure tHisA protein per gram of wet cell mass. The t*trp*F gene variants were heterologously expressed in *E. coli*, and the host cells from a 37 L fermenter were lysed by sonification and treated with heat as described previously (*11*, *18*). The centrifuged supernatant after the heat treatment was dialyzed against 50 mM Tris-HCl (pH 7.5), 2 mM EDTA, and 1 mM DTT and loaded on a DEAE-Sephacel column (5 cm × 29.5 cm, Pharmacia) that was equilibrated with the same buffer, at 4 °C. The column was washed with 2 volumes of equilibration buffer, and bound proteins were eluted with 3 L of a linear gradient of 0 to 350 mM NaCl, without EDTA. Fractions containing tTrpF were pooled and loaded on a hydroxyapatite column (3.5 cm × 22.6 cm), which was equilibrated with 50 mM Tris-HCl (pH 7.5) and 1 mM DTT. The column was washed with 3 volumes of the same buffer, and bound proteins were eluted with 1.4 L of a linear gradient of 0 to 200 mM potassium phosphate (pH 7.5). The fractions containing tTrpF were pooled, dialyzed against 20 mM potassium phosphate (pH 7.5), 1 mM DTT, and 1 mM EDTA, concentrated by ultrafiltration to 20−25 mg/mL, and stored through shock

freezing in liquid nitrogen. The yields were between 0.34 and 0.68 mg of pure tTrpF protein per gram of wet cell mass.

In Vivo Complementation. The t*his*A gene variants were subcloned from pDS56/RBSII into pTNA, which contains a truncated derivative of the tryptophanase operon promoter that permits constitutive gene expression in *E. coli* (*13*, *19*). The auxotrophic *E. coli* strain HfrG6 (*20*), which carries a mutant e*his*A gene that encodes an inactive eHisA protein, was transformed with the various pTNA-t*his*A plasmids, plated on ampicillin-containing minimal medium plates (*21*) without histidine, and incubated at 37 °C.

Crystallization and X-ray Structure Determination of the Complex between tTrpF and Its Product Analogue, Reduced 1-[(2-Carboxyphenyl)amino]-1-deoxyribulose 5-Phosphate (rCdRP). Crystallization was performed using the hanging drop vapor diffusion method. In a vapor diffusion experiment, drops containing 5 μL of a 19 mg/mL tTrpF protein solution were mixed with 5 μL of reservoir solution [0.1 M MES buffer (pH 7.0) containing 1.5 M ammonium sulfate]. Crystals were first observed ~3 days after setting up the drops, and were allowed to grow for at least 2 weeks. Their maximum dimensions were 0.2 mm × 0.2 mm × 0.5 mm. Subsequently, the crystals were soaked in a solution of 0.1 M MES buffer (pH 7.0) containing 1.6 M ammonium sulfate. The concentration of rCdRP was in a stepwise fashion increased from 0.1 to 1.2 mM by exchange of the soaking solution. Crystals were mounted in glass capillaries and X-ray data were measured on a modified Marconi-Elliott GX-20 rotating anode generator with a copper anode operated at 40 kV and 50 mA. The data were evaluated with the MOSFLM program package (*22*). Phases were obtained using the refined structure of tTrpF (*23*), without solvent molecules (water and phosphate ion), as the starting model for difference Fourier methods. All reflections, without application of a σ cutoff, were used in the refinement of the structure. After several cycles of restrained positional and individual temperature factor refinement using XPLOR (*24*), the molecular structure was inspected and rebuilt with the molecular graphics program O (*25*), using SIGMAA-weighted $F_o - F_c$ and $2F_o - F_c$ electron density maps (*26*).

Analytical Methods. Purification of proteins was followed by electrophoresis on 12.5 or 15% SDS−polyacrylamide gels using the system of Laemmli (*27*) and staining with Coomassie Blue. During purification, the protein concentration was determined according to the method of Bradford (*28*). The concentration of purified proteins was determined by absorption spectroscopy at 280 nm with molar extinction coefficients that were determined by second-derivative spectroscopy (*29*) or calculated from the amino acid sequence (*30*). Sedimentation equilibrium runs in a Beckman analytical ultracentrifuge (model Optima XL A) were performed with eHisA and tHisA at 20 °C and 23000−26000 rpm. The initial protein concentrations were between 0.3 and 0.6 mg/mL in 50 mM potassium phosphate buffer (pH 7.5) containing between 0.4 and 1 mM DTT and EDTA and either 700 mM NaCl (eHisA) or 150 mM NaCl (tHisA). The absorption was followed at 226 or 277 nm, and the runs were analyzed by a self-written computer program that adjusts the baseline absorbance (A) to obtain the best linear fit of ln A versus the square of the radial distance (r^2). An assumed partial specific volume of 0.73 mL/g was used to determine the molecular masses. Analytical gel filtration of the tHisA variants was performed at a flow rate of 0.5 mL/min on a calibrated Superdex 75 column (1 cm × 30 cm, Amersham Pharmacia Biotech) that was equilibrated with 50 mM potassium phosphate (pH 7.5) containing 300 mM sodium chloride and 1 mM DTT.

Steady-State Enzyme Kinetics and Ligand Titration. The isomerization of ProFAR into *N*′-[(5′-phosphoribulosyl)-formimino]-5-aminoimidazole-4- carboxamide ribonucleotide (PRFAR) catalyzed by eHisA and tHisA was followed at various temperatures, using 50 mM Tris-HCl containing 1 mM EDTA and 1 mM DTT. The pH was adjusted at 25 °C to a value that corresponded to a value of 7.5 at the respective temperature, assuming a ΔpK_a/°C for Tris buffer of −0.028 (*31*). The presence of a sufficient excess of both glutamine and the imidazole glycerol phosphate (ImGP) synthase from *T. maritima* [1:1 complex of the glutaminase subunit tHisH and the synthase subunit tHisF (*13*)] led to a rapid conversion of the product PRFAR into ImGP and 5-aminoimidazole-4-carboxamide ribotide (AICAR), which prevented product inhibition and allowed us to use the decrease in absorbance at 300 nm to monitor the reaction [$\Delta\epsilon_{300}$(PRFAR − AICAR) = 5.637 mM^{-1} cm^{-1} (*7*)]. Entire progress curves were recorded and analyzed with the integrated form of the Michaelis−Menten equation using the program COSY (*32*, *33*) to obtain k_{cat} and K_M^{ProFAR}. The isomerization of PRA into 1-[(2-carboxyphenyl)amino]-1-deoxyribulose 5-phosphate (CdRP) catalyzed by the tTrpF variants was followed at 25 °C with a fluorimetric assay (*33*), using 50 mM Tris-HCl (pH 7.5) containing 2 mM EDTA and 1 mM DTT. The dependence of initial velocities on the substrate concentration was recorded and analyzed with the direct linear plot method (*34*). The binding of the substrate PRA and the product analogue rCdRP to tTrpF_C7A_D126N was followed by fluorescence energy transfer (*11*, *33*, *35*) in 50 mM potassium phosphate buffer (pH 7.5) containing 1 mM EDTA and 0.5 mM DTT.

Stability Measurements of eHisA, tHisA, and ProFAR. The irreversible loss of the circular dichroism (CD) signal in the far-UV region after incubation at various temperatures was used as an operational criterion of the thermostability of eHisA and tHisA. Stock solutions of the proteins were diluted to final concentrations of 24−27 μM into prewarmed and degassed 50 mM potassium phosphate buffer (pH 7.5) containing 1 mM EDTA and 1.5 mM DTT. The samples were overlaid with mineral oil to prevent evaporation and incubated for 10 min in a heating block (Biometra, Trio Thermoblock) at the respective temperatures, and then put on ice and centrifuged to remove the precipitant. The soluble protein in the supernatant was diluted 3-fold with 50 mM potassium phosphate (pH 7.5). The residual CD signal at 222 nm was then monitored at 22 °C for 3 min, and the obtained averaged values were plotted against the incubation temperature.

ProFAR hydrolyzes spontaneously in a single-exponential process that can be followed by a decrease in absorption at 300 nm (*10*). It has been shown by HPLC, UV spectroscopy, and ^{1}H NMR that one degradation product is AICAR. A second degradation product could not be characterized, because it further decomposed during purification attempts (*10*). The rate of ProFAR hydrolysis at 37, 60, and 80 °C was measured in 50 mM Tris-HCl buffer (pH 7.5) containing 1 mM EDTA and 1 mM DTT. The pH was adjusted at 25

°C to a value that corresponded to a value of 7.5 at the respective temperature, assuming a ΔpK_a/°C for Tris buffer of −0.028 (*31*). To exclude any influence of Tris buffer on the degradation kinetics, ProFAR hydrolysis at 60 °C was also monitored in 50 mM potassium phosphate (pH 7.5). The measured first-order degradation rates were identical for the two buffer systems.

RESULTS AND DISCUSSION

Production and Purification of the tHisA and tTrpF Variants, and of eHisA. The tHisA protein and its variants tHisA_D8N, _H48A, _D51N, _R83N, _D127N, and _T164A as well as tTrpF variants tTrpF_C7A, _D126N, and _C7A_D126N were produced by expressing the corresponding genes in *E. coli*. The soluble crude extract was heated to denature most host proteins, which were removed by centrifugation. The second purification step involved affinity chromatography on Red Sepharose in the case of the tHisA variants, and both anion exchange and hydroxyapatite chromatography in the case of the tTrpF variants. The eHisA protein was produced in *E. coli* with an N-terminal hexahistidine tag of 16 amino acid residues, which allowed us to use metal chelate affinity chromatography as the first purification step. Residual protein contaminants were removed by hydroxyapatite chromatography. Attempts to cleave off the N-terminal histidine tag of eHisA proteolytically were not successful and resulted in a considerable loss of enzymatic activity. For this reason and because several proteins with and without the N-terminal His tag had identical enzymatic and ligand binding properties (*36*, *37*), all further investigations were performed with eHisA that contained the N-terminal extension. Sedimentation equilibrium runs in the analytical ultracentrifuge yielded apparent molecular masses of 25.6 kDa for wild-type tHisA and 27.4 kDa for eHisA, which are close to the calculated molecular masses of 27.0 and 28.2 kDa, respectively, for the monomers (data not shown). Analytical gel filtration on a calibrated Superdex 75 column confirmed that tHisA and all of its variants are monomers (data not shown). In contrast, tTrpF and its variants are dimers with a calculated molecular mass of ∼46.1 kDa (*11*). The concentrations of the purified variants were determined by absorption spectroscopy, using calculated molecular extinction coefficients at 280 nm (*30*) of 12 950 M^{-1} cm^{-1} for monomeric tHisA and 25 440 M^{-1} cm^{-1} for monomeric eHisA. The molecular extinction coefficient of dimeric tTrpF was determined to be 27 860 M^{-1} cm^{-1}, using second-derivative spectroscopy (*29*).

Thermostabilities of eHisA, tHisA, and ProFAR. The thermal stabilities of eHisA and tHisA at pH 7.5 were measured by following the decrease in the magnitude of the CD signal at 222 nm after a 10 min incubation at various temperatures. Under these conditions, eHisA and tHisA display half-denaturation temperatures (50% loss of the initial CD signal) of 40 and 95 °C, respectively (data not shown). The kinetic stability of the substrate of HisA, ProFAR, was investigated at pH 7.5 and various temperatures (37, 60, and 80 °C) and in various buffer systems (Tris-HCl and potassium phosphate) by following the rate of the decrease in absorbance at 300 nm. The decomposition of ProFAR is an exponential process with the following half-lives (first-order rate constants): 953 min (1.2×10^{-5} s^{-1}) at 37 °C, 75 min (1.5×10^{-4} s^{-1}) at 60 °C, and 13 min (8.8×10^{-4} s^{-1}) at 80 °C. The rate of ProFAR hydrolysis was independent of the buffer system (Tris-HCl or potassium phosphate) that was used.

Table 1: Temperature Dependence of the Steady-State Kinetic Constants of eHisA and tHisA[a]

enzyme	T (°C)	k_{cat} (s^{-1})	K_M^{ProFAR} (μM)	k_{cat}/K_M^{ProFAR} (μM^{-1} s^{-1})
eHisA	25	4.9	1.6	3.1
	37	14.3	1.8	7.9
tHisA	25	0.67	0.6	1.1
	37	1.54	0.6	2.6
	80	32.0	<1[b]	>32[b]

[a] The standard errors on all constants are less than ±20%. Conditions: 50 mM Tris-HCl, pH 7.5 at the corresponding temperature, 1 mM EDTA, 1 mM DTT, 5 mM glutamine, and 2 μM tHisF−tHisH complex. [b] The quality of the data at 80 °C only allowed determination of an upper limit for K_M^{ProFAR} and a lower limit for k_{cat}/K_M^{ProFAR}.

Temperature Dependence of the Catalytic Efficiencies of Wild-Type tHisA and eHisA. For the determination of the catalytic efficiencies of eHisA and tHisA at various temperatures, entire progress curves of the conversion of ProFAR to PRFAR were recorded and fitted to the integrated form of the Michaelis−Menten equation (*7*, *32*, *33*). The results are summarized in Table 1. The value of the catalytic efficiency parameter k_{cat}/K_M^{ProFAR} is ∼3-fold higher for eHisA than for tHisA, at both 25 and 37 °C. However, when compared at the corresponding physiological growth temperatures of *E. coli* and *T. maritima*, tHisA (>32 μM^{-1} s^{-1} at 80 °C) is at least 4-fold more efficient than eHisA (7.9 μM^{-1} s^{-1} at 37 °C). Similarly, tTrpF at 80 °C is ∼8-fold more efficient than eTrpF at 37 °C (*11*). In contrast, most orthologous enzymes from hyperthermophiles and mesophiles have comparable efficiencies at their corresponding physiological temperatures. This phenomenon of "corresponding states" (*38*) is probably due to a similar conformational flexibility of mesophilic and thermophilic enzymes at the optimal growth temperature of their respective hosts (*39*). The physiological rationale for the relatively large catalytic efficiency of tHisA might be to outrun the decay of its thermolabile substrate ProFAR. This hypothesis was tested by comparing the rate of catalytic conversion of ProFAR by HisA (v_c) to the rate of its hydrolysis (v_h) under physiological temperatures, following previous procedures developed for TrpF (*11*):

$$v_c/v_h = [(k_{cat}/K_M^{ProFAR})/k_h][E_0]$$

where k_h is the first-order rate constant of ProFAR hydrolysis.

We assume that the intracellular concentration of eHisA monomers is ∼2 μM in derepressed cells (*40*). Under these conditions, and with the measured values at 37 °C of k_{cat}/K_M^{ProFAR} (7.9 μM^{-1} s^{-1}) of eHisA and k_h (1.2×10^{-5} s^{-1}), $v_c/v_h \sim 1.3 \times 10^6$ (Table 2). From the values at 80 °C of k_{cat}/K_M^{ProFAR} (>32 μM^{-1} s^{-1}) of tHisA and k_h (8.8×10^{-4} s^{-1}), $v_c/v_h > 6.4 \times 10^4$ (Table 2). As shown previously for eTrpF and tTrpF (*11*), these large values of the "competition quotients" v_c/v_h document that eHisA and tHisA also convert their labile substrate to a useful product far more rapidly than it decays spontaneously (Table 2).

The extremely thermostable enzymes TrpF and HisA from *T. maritima* are at room temperature comparably as efficient as their thermolabile orthologues from *E. coli* (Table 1). These findings show that high enzymatic efficiency at low

Table 2: Competition between Spontaneous Hydrolysis and Productive Processing of the HisA Substrate ProFAR and the TrpF Substrate PRA[a]

enzyme	T (°C)	k_h (s^{-1})[c]	k_{cat}/K_M (μM^{-1} s^{-1})	v_c/v_h[d]
eHisA	37	1.2×10^{-5}	7.9	$\sim 1.3 \times 10^6$
eTrpF[b]	37	2.4×10^{-3}	3.3	$\sim 2.8 \times 10^3$
tHisA	80	8.8×10^{-4}	>32	$>6.4 \times 10^4$
tTrpF[b]	80	1.7×10^{-2}	113.4	$\sim 1.5 \times 10^4$

[a] The standard errors on all constants are less than ±20%. [b] Data from ref *11*. [c] First-order rate constant of substrate hydrolysis at the given temperature. [d] Ratio of catalytic to hydrolysis rates at an assumed intracellular enzyme concentration of 2 μM (*40*).

temperatures and high thermostability are not mutually exclusive properties. Along these lines, novel enzymes that display a similar combination of properties were recently generated by rational protein design and directed evolution techniques (*41*−*43*). This combination of properties is rarely found in native enzymes, probably due to a lack of selective pressure, since enzymes from mesophiles do not require high thermostability, and the catalytic efficiencies of hyperthermophilic enzymes normally need not be high at low temperatures (*43*, *44*).

Identification of Catalytically Essential Residues in tHisA and tTrpF. The catalytic residues are expected to be invariant in all known HisA sequences, and to be located at the C-terminal face of the central β-barrel of tHisA, where the active sites of all known $(\beta\alpha)_8$-barrel enzymes are found (*2*, *3*). Catalytic residues should also donate or accept a proton, since the HisA reaction probably involves general acid−base catalysis. Six residues that fulfill most of these criteria were replaced by site-directed mutagenesis with structurally similar residues lacking the putative functional group (Figure 2). The steady-state kinetic constants of the purified tHisA variants were compared with the constants of the wild-type enzyme (Table 3). The catalytic efficiencies k_{cat}/K_M^{ProFAR} of tHisA_H48A, tHisA_D51N, tHisA_R83N, and tHisA_T164A are only ∼10−350-fold smaller than the k_{cat}/K_M^{ProFAR} of wild-type tHisA, ruling out an essential catalytic role for the replaced residues. However, Arg83 appears to be important for substrate binding, because K_M^{ProFAR} of tHisA_R83N is increased ∼60-fold compared to that of the wild-type enzyme. In contrast, the residual activity of tHisA_D8N was too low to be measured even in the presence of high enzyme concentrations (50 μM), and the catalytic efficiency of tHisA_D127N was decreased by almost 4 orders of magnitude, mostly due to a drastic reduction in k_{cat}.

To further investigate the role of the exchanged amino acid residues for catalysis of the HisA reaction, we tested the ability of the tHisA variants to complement the *his*A deficiency of an auxotrophic *E. coli* strain. Cells that were transformed with the plasmid-encoded mutants t*his*A_D8N and t*his*A_D127N did not form visible colonies on selective plates lacking histidine, even after a 1 week incubation at 37 °C. In contrast, transformation with t*his*A_T164A resulted

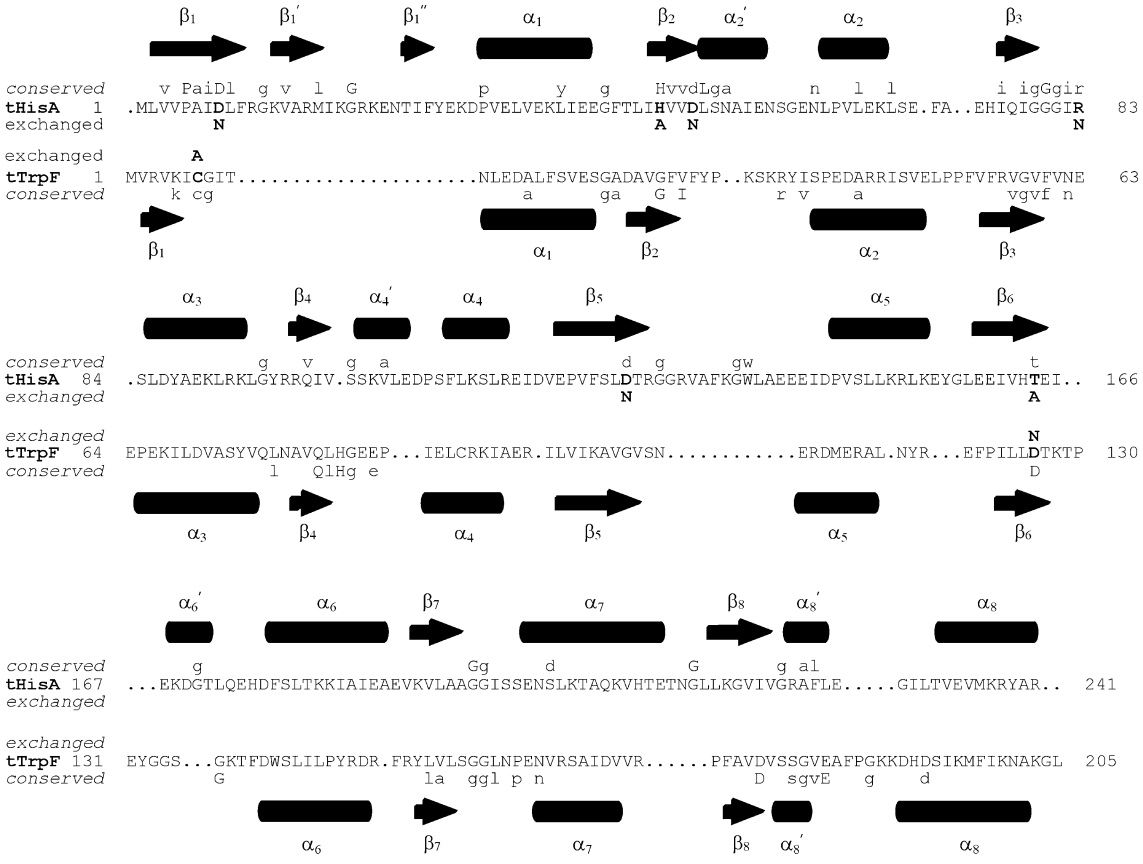

FIGURE 2: Conserved and putative essential amino acid residues within $(\beta\alpha)_8$-barrel enzymes tHisA and tTrpF. A structure-based sequence alignment between tHisA and tTrpF is shown (*7*). β-Strands are identified with arrows and α-helices with cylinders. Conserved residues are depicted in uppercase letters for invariant residues in 24 HisA or 40 TrpF sequences and in lowercase letters for residues conserved in at least 90% of the HisA or TrpF sequences. For exchanged residues, six invariant or conserved residues in the active site of tHisA and two invariant residues in the active site of tTrpF were replaced individually with structurally similar residues (in boldface).

Table 3: Steady-State Enzyme Kinetic Constants for Wild-Type (WT) and Mutant tHisA and tTrpF Enzymes[a]

	WT tHisA[b]	D8N tHisA[b]	H48A tHisA[b]	D51N tHisA[b]	R83N tHisA[b]	D127N tHisA[b]	T164A tHisA[b]
k_{cat} (s^{-1})	0.67	ND[e]	0.38	0.29	0.23	0.00027	0.018
K_m^{ProFAR} (μM)	0.60	ND[e]	2.9	6.4	37.9	2.0	5.6
k_{cat}/K_m^{ProFAR} (μM^{-1} s^{-1})	1.1	ND[e]	0.131	0.046	0.006	0.00013	0.003

	WT[c] tTrpF[d]	C7A tTrpF[d]	D126N tTrpF[d]
k_{cat} (s^{-1})	3.7	ND[e]	<0.001
K_m^{PRA} (μM)	0.28	ND[e]	2.1
k_{cat}/K_m^{PRA} (μM^{-1} s^{-1})	13.3	ND[e]	<0.0005

[a] The standard errors for all constants are less than ±20%. [b] Conditions: 50 mM Tris-HCl, pH 7.5 at 25 °C, 1 mM EDTA, 1 mM DTT, 1 μM tHisF−tHisH complex, 5 mM glutamine, and between 0.2 (WT) and 50 μM (D8N) tHisA. Exchange at the following positions: β1, β2, β2, loop β3α3, β5, and β6 for D8N, H48A, D51N, R83N, D127N, and T164A, respectively. [c] Data from ref *11*. [d] Conditions: 50 mM Tris-HCl, pH 7.5 at 25 °C, 2 mM EDTA, 1 mM DTT, and between 1.4 nM (WT) and 15 μM (C7A) tTrpF. Exchange at the following positions: β1 for C7A and β6 for D126N. [e] Not determined, since the activity was immeasurably low. The same is true for the double mutant tTrpF_C7A_D126N.

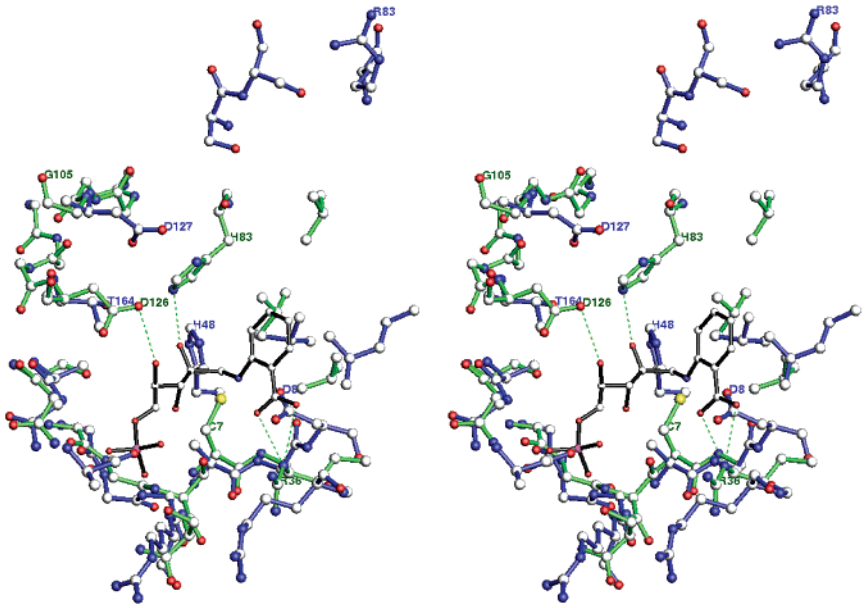

FIGURE 3: Superposition (stereoview) of the active sites of tTrpF (green sticks) with bound product analogue rCdRP (black sticks) and tHisA (blue sticks) without bound ligand. Carbon atoms are depicted in gray, oxygen atoms in red, and nitrogen atoms in blue; the sulfur atom of Cys7 is depicted in yellow and the phosphorus atom of rCdRP in pink. Dashed lines represent a salt bridge between the side chain of Arg36 and the carboxylate group of the anthranilate moiety of rCdRP (Nϵ−O distances of 2.8 and 3.1 Å), a hydrogen bond between the imidazole group of His83 and the C2′-hydroxyl oxygen of rCdRP (N−O distance of 2.8 Å), and a hydrogen bond between the carboxylate side chain of Asp126 and the C4′-hydroxyl oxygen of rCdRP (O−O distance of 3.0 Å). The sulfhydryl group of Cys7 from tTrpF is located close to the C2′ atom of rCdRP (S−C distance of 3.9 Å). With respect to potentially equivalent catalytic residues of tTrpF and tHisA, Asp126 (β-strand 6 in tTrpF) and Asp127 (β-strand 5 in tHisA) probably act as general acids and Cys7 (β-strand 1 in tTrpF) and Asp8 (β-strand 1 in tHisA) probably act as general bases (cf. Figure 4). The superposition was performed with MOLOC (*53*).

in visible colonies after 2 days, and all other tHisA variants, including the wild-type enzyme, complemented the *his*A deficiency overnight. Thus, the complementation experiments in vivo qualitatively confirm the steady-state measurements in vitro, proving that Asp8 and Asp127 are essential, and that Thr164 is important for catalysis of the HisA reaction. Moreover, it appears that the K_M^{ProFAR} is irrelevant for complementation, since no time difference in colony growth was observed between tHisA_R83N and the wild-type enzyme, although K_M^{ProFAR} was increased significantly by the introduced amino acid exchange (Table 3). Most likely, ProFAR accumulates in the *his*A deficiency strain, thus saturating even the variants with increased K_M^{ProFAR} values, making k_{cat} the selected trait in our experiments (*7*).

The important amino acids (Asp8, Asp127, and Thr164) of tHisA are located at the C-terminal ends of β-strands 1, 5, and 6, respectively (Figure 2). It is plausible to assume that the location of catalytic residues is conserved between tHisA and tTrpF. The invariant Cys7 of tTrpF is located at the C-terminal end of β-strand 1 and is equivalent to Asp8 of tHisA; the invariant Asp126 of tTrpF is located at the C-terminal end of β-strand 6 and is equivalent to Thr164 of tHisA, but also close in space to Asp127 at the C-terminal end of β-strand 5 (Figures 2 and 3). Therefore, to reveal their importance for catalysis, Cys7 and Asp126 of tTrpF were replaced individually and together by site-directed mutagenesis, and the steady-state kinetic constants of the purified tTrpF variants tTrpF _C7A, tTrpF_D126N, and tTrpF_C7A_D126N were compared with those of wild-type tTrpF (Table 3). Whereas the residual activities of tTrpF_C7A and tTrpF_C7A_D126N were too low to be detected, the catalytic efficiency k_{cat}/K_M^{PRA} of tTrpF_D126N was decreased at least 20000-fold compared to that of the wild-type enzyme.

Ligand Binding Studies of tTrpF Variants with rCdRP and PRA. Since tTrpF_C7A_D126N has no detectable enzymatic

Table 4: Data for the X-ray Data Collection and Refinement of the tTrpF−rCdRP Complex

resolution range (Å)	20.0−2.80
no. of measured reflections	28569
no. of unique reflections	6978
completeness (%)	99.3
R_{sym} (%)[a]	9.9
no. of protein atoms	1548
no. of waters	8
no. of ligand atoms	23
rmsd for distances (Å)	0.010
rmsd for bond angles (deg)	1.8
R_{factor} at start of refinement (%)[b]	35.3
R_{work} at end of refinement (%)[b]	17.0
R_{free} at end of refinement (5% of data, %)[b]	22.8
mean *B*-factor for proteins (Å^2)	27.0
mean *B*-factor for ligands (Å^2)	32.0
mean *B*-factor for waters (Å^2)	36.4

[a] $R_{sym} = \sum_{hkl}\sum_i|I(hkl)_i - \langle I(hkl)\rangle|/\sum_{hkl}\sum_i\langle I(hkl)_i\rangle$. [b] $R_{factor} = \sum_{hkl}|F(hkl)_o - F(hkl)_c|/\sum_{hkl}F(hkl)_o$.

activity, this variant offers the possibility of determining the affinity of binding to the true substrate PRA by fluorescence energy transfer (*11*, *33*, *35*). The spontaneous decay of PRA (cf. Table 2) was compensated by its constant resynthesis in situ from anthranilate and a 10-fold molar excess of PRPP catalyzed by anthranilate phosphoribosyl transferase from yeast (*11*, *33*). The titrations yielded an isoemissive point at 364 nm (data not shown), indicating that only one mode of binding of PRA to a specific binding site is involved. The binding occurred with the expected stoichiometry of 2 mol of PRA per mole of dimeric tTrpF_C7A_D126N and yielded a K_d^{PRA} of 0.21 μM. The binding of the product analogue rCdRP (Figure 1) to tTrpF_C7A_D126N was followed by fluorimetric titration. The titration yielded an isoemissive point at 378 nm (data not shown), indicating that only one mode of binding of rCdRP to a specific binding site is involved. The binding occurred with the expected stoichiometry (2 mol of rCdRP per mole of dimeric tTrpF_C7A_D126N) in a noncooperative manner and with a K_d^{rCdRP} of 0.03 μM, which is 17-fold smaller than that for wild-type tTrpF (*11*). Because the binding of rCdRP and PRA results in different isoemissive points, the microenvironment of the anthranilate ring of these two ligands within the active site of tTrpF_C7A_D126N must be different.

X-ray Structure Analysis of the Complex between tTrpF and Its Product Analogue rCdRP. To gain more insight into the reaction mechanism of tHisA and tTrpF, we attempted to obtain crystals of either of the enzymes with a ligand bound to the active site. Unfortunately, no stable substrate or product analogue is presently available for tHisA. Co-crystallization of the inactive tHisA_D8N variant (Table 3) with the true substrate ProFAR failed, probably due to the instability of ProFAR (Table 2). It was possible, however, to obtain crystals of tTrpF complexed with its product analogue rCdRP (Figure 1), which, as shown by fluorescence titration, binds with high affinity (*11*). Details about the data collection and the refinement parameters are summarized in Table 4. The structure of the tTrpF−rCdRP complex at a resolution of 2.8 Å, superimposed with the structure of tHisA without a bound ligand (*45*), is depicted in Figure 3. It shows that the side chain of the conserved residue of tTrpF (Arg36) forms a salt bridge with the carboxylate group of the

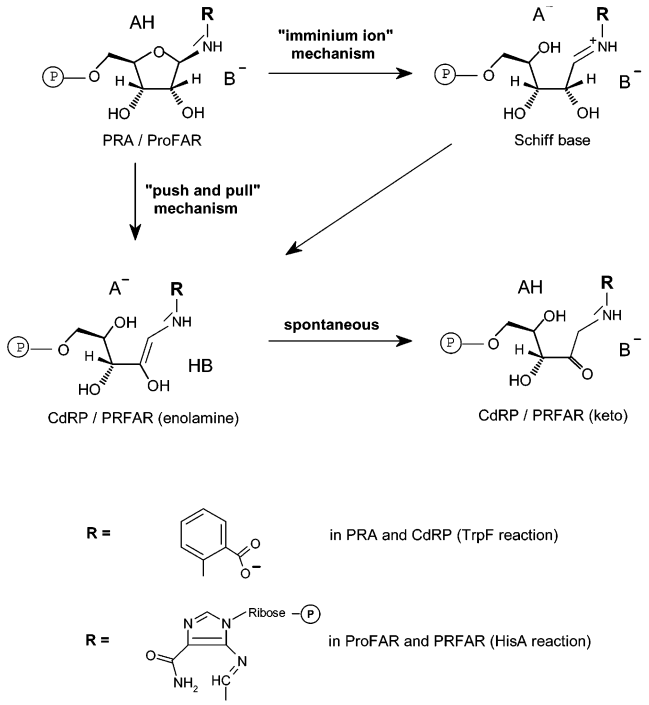

FIGURE 4: Plausible mechanism of the Amadori rearrangements catalyzed by tTrpF and tHisA. In tTrpF, the general acid AH and the general base B^- are probably identical to Asp126 and Cys7, respectively; in tHisA, the most likely candidates for AH and B^- are Asp127 and Asp8, respectively (cf. Figure 3 and see the text for details).

anthranilate moiety of rCdRP (Nϵ−O1 distance of 2.8 Å, Nϵ−O2 distance of 3.1 Å). The oxygen atom of the carboxylate group of the invariant residue Asp126 hydrogen bonds to the C4′-hydroxyl oxygen of rCdRP (O−O distance of 3.0 Å), which corresponds to the furanose ring oxygen of the substrate PRA. The sulfhydryl group of the conserved residue Cys7 is located close to the C2′ atom of rCdRP (S−C distance of 3.9 Å), which corresponds to the C2′ atom of PRA. The analysis of the electron density suggests that the absolute configuration at the C2′ atom of rCdRP is "*S*" in its complex with tTrpF. In contrast, the absolute configuration at the same C2′ atom of rCdRP is "*R*" in its complex with indole-3-glycerol phosphate synthase from *Sulfolobus solfataricus* (sTrpC), which is the enzyme that catalyzes the subsequent reaction in the biosynthesis of tryptophan (*46*). These differences in diastereomer binding are likely due to specific hydrogen bonding between the C2′-hydroxyl oxygen of rCdRP, which takes place with His83 in tTrpF [N−O distance of 2.8 Å (Figure 3)] and with Lys110 in sTrpC [N−O distance of 2.5 Å (*46*)].

Catalytic Mechanism of HisA and TrpF. HisA and TrpF are $(\beta\alpha)_8$-barrel enzymes which catalyze analogous Amadori rearrangements of a phosphorylated aminoaldose into the corresponding aminoketose (Figure 1). It is plausible, therefore, to assume that the two enzymes use similar catalytic mechanisms. Figure 4 shows a putative reaction mechanism which involves general acid−base catalysis. In the first step, the furanose ring oxygen of PRA (TrpF) or ProFAR (HisA) is protonated by the general acid AH, yielding a Schiff base ("imminium ion") intermediate. A proton is then abstracted from the C2′ atom of the ribose by the general base B^- to yield the enolamine form of CdRP (TrpF) or PRFAR (HisA). Alternatively, the enolamine could

be generated in a single step by a "push and pull mechanism", which would require the general acid and the general base to act simultaneously (*47*). The subsequent conversion of the enolamine form of CdRP to the keto form occurs spontaneously in the case of TrpF. It is independent of the enzyme concentration (*33*). Anthranilate and ribose 5-phosphate combine spontaneously in the presence of 50% ethanol, yielding PRA, which tautomerizes spontaneously to CdRP (*48*, *49*). Ammonia and ribose 5-phosphate also combine spontaneously to form phosphoribosylamine, but the analogous condensation of ammonia with just ribose occurs far more slowly (*50*). This observation suggests that the phosphate group performs intramolecular catalysis. By analogy, the phosphate group of PRA could be enrolled for substrate-assisted catalysis in the active site of tTrpF. As shown in Figure 4, however, the phosphate group of rCdRP is too far removed from either the C4′-hydroxyl group or the C2′ atom to qualify as a general acid or general base.

In contrast, the loss of catalytic activity of the tTrpF_C7A variant and the drastic reduction of the k_{cat} value of the tTrpF_D126N variant (Table 3), as well as the structure of the tTrpF−rCdRP complex (Figure 3) suggest that Cys7 and Asp126 may act as the general base and general acid, respectively. In support of this hypothesis, the pK_a of the SH group of the corresponding Cys residue in eTrpF is <6.8 (*51*), which would allow proton abstraction from the C2′ atom of PRA at physiological pH values. In contrast, the side chain carboxylate of Asp126 must be uncharged to protonate the furanose ring oxygen of PRA, and therefore, its pK_a value must be increased by several units compared to that of free aspartate. This assumption is supported by the inspection of the tTrpF structure. Among the eight nearest-neighbor residues (threshold of 6 Å) of Asp126 (His83, Val104, Gly105, Leu124, Leu125, Thr127, Ser157, and Gly158), five are hydrophobic, making the deprotonation of its side chain energetically unfavorable. A second function of Asp126 could be the stabilization of the proposed imminium intermediate on the reaction pathway (Figure 4), but the large distance of 6.4 Å between the carboxylate group of Asp126 and the nitrogen atom of anthranilate in the tTrpF−rCdRP complex does not support this possibility. As shown by fluorimetric titration (see above), the simultaneous replacement of Cys7 with Ala and of Asp126 with Asn decreases the thermodynamic dissociation constant of the product analogue rCdRP almost 20-fold. This result suggests that the newly introduced residues bind more tightly to the product CdRP than the wild-type residues. Thus, Cys7 and Asp126 not only may be involved in the catalytic process but also could accelerate the dissociation of the enolamine form of CdRP from the enzyme, which is then converted to the keto form in solution (*33*).

Without the structure of a tHisA−ligand complex, only circumstantial evidence exists for the specific roles of Asp8, Asp127, and Thr164 in tHisA. It seems plausible to assume that structurally equivalent residues are used for catalysis in tTrpF and tHisA. Accordingly, Asp8 of tHisA, which is equivalent to Cys7 of tTrpF, would act as general base, and Thr164 or Asp127 of tHisA, each of which is equivalent to Asp126 of tTrpF (Figures 2 and 3), would act as general acid in the tHisA reaction. Since it seems rather improbable that the hydroxyl side chain of Thr164 could provide a proton for catalysis, it is likely that Asp127 is the general acid. Consequently, Asp126 of tTrpF and Asp127 of tHisA would be located on different β-strands but nevertheless perform the same function, as was observed for essential residues of $(\beta\alpha)_8$-barrel enzymes from the enolase superfamily (*1*).

CONCLUSION

Several similarities motivated us to study HisA and TrpF in parallel. Both enzymes have the $(\beta\alpha)_8$-barrel fold and catalyze Amadori rearrangements in two independent aromatic amino acid biosynthesis pathways. Moreover, both HisA and TrpF must have evolved mechanisms for circumventing the lability of their substrates ProFAR and PRA, the elucidation of which is generally interesting and also facilitated by the availability of both the mesophilic enzyme variants from *E. coli* and the hyperthermophilic ones from *T. maritima*. The results presented here suggest that the loss of the labile substrates is prevented by their rapid catalytic turnover rather than by channeling between the enzymes by which they are produced or consumed. To suppress the decay of the substrates with comparable efficiency, the HisA and TrpF variants from *T. maritima* display a significantly higher catalytic efficiency at 80 °C than their homologues from *E. coli* at 37 °C. The thermostable forms of HisA and TrpF possess, moreover, significant catalytic efficiency also at moderate temperatures. This observation was not expected, as most enzymes from hyperthermophiles are only very weakly active at ambient temperatures, probably due to structural rigidity that ensures high stability but at the same time prevents conformational transitions that are necessary for efficient catalysis (*52*). Since both HisA and TrpF from *T. maritima* are extremely thermostable, it follows either that the relatively simple Amadori reaction catalyzed by HisA and TrpF does not require major conformational rearrangements or that structural flexibility in these enzymes is restricted to the active sites.

A plausible reaction mechanism of the Amadori rearrangements catalyzed by HisA and TrpF involves general acid−base catalysis (Figure 4). The replacement of invariant amino acids at the C-terminal faces of the central β-barrels identifies three functionally important residues in HisA, namely, Asp8, Asp127, and Thr164, and two functionally important residues in TrpF, namely, Cys7 and Asp126 (Figure 2). The X-ray structure of the complex between TrpF and the product analogue rCdRP (Figure 3) assigns Asp126 as the general acid, which protonates the furanose ring oxygen, and Cys7 as the general base, which abstracts a proton from the C2′ atom of the ribose. The specific roles of the essential residues of HisA are less clear, but by analogy with tTrpF, Asp127 would be the general acid and Asp8 the general base. Interestingly, the replacement of Cys7 in tTrpF, Asp8 in tHisA, and Asp11 in tHisF, a $(\beta\alpha)_8$-barrel enzyme that catalyzes the subsequent step in histidine biosynthesis and displays residual HisA activity (*45*), results in the complete inactivation of the three enzymes. Cys7, Asp8, and Asp11 are located at equivalent positions at the C-terminal ends of β-strand 1 of each enzyme. In contrast, the replacement of Asp126 in tTrpF, Asp127 in tHisA, and Asp130 in tHisF, which are located at the C-terminal ends of β-strand 5 or 6, results in a significantly reduced but still measurable k_{cat} value (Table 3 and ref *13*). The structural conservation

of the only absolutely essential amino acid residue among tTrpF, tHisA, and tHisF supports the hypothesis that these three $(\beta\alpha)_8$-barrel enzymes of aromatic amino acid biosynthesis have evolved from a common ancestor (*6*).

ACKNOWLEDGMENT

We thank Ariel Lustig for running the analytical ultracentrifuge and Drs. Hans-Joachim Fritz, Harald Kolmar, and Wilfried Kramer (Georg-August-Universität Göttingen) for continuous support and discussions.

REFERENCES

1. Gerlt, J. A., and Babbitt, P. C. (2001) Divergent Evolution of Enzymatic Function: Mechanistically Diverse Superfamilies and Functionally Distinct Suprafamilies, *Annu. Rev. Biochem. 70*, 209−246.
2. Wierenga, R. K. (2001) The TIM-barrel fold: a versatile framework for efficient enzymes, *FEBS Lett. 492*, 193−198.
3. Höcker, B., Jürgens, C., Wilmanns, M., and Sterner, R. (2001) Stability, catalytic versatility and evolution of the $(\beta\alpha)_8$-barrel fold, *Curr. Opin. Biotechnol. 12*, 376−381.
4. Copley, R. R., and Bork, P. (2000) Homology among $(\beta\alpha)_8$ Barrels: Implications for the Evolution of Metabolic Pathways, *J. Mol. Biol. 303*, 627−640.
5. Babbitt, P. C., and Gerlt, J. A. (2000) New functions from old scaffolds: how nature reengineers enzymes for new functions, *Adv. Protein Chem. 55*, 1−28.
6. Henn-Sax, M., Höcker, B., Wilmanns, M., and Sterner, R. (2001) Divergent Evolution of $(\beta\alpha)_8$-barrel enzymes, *Biol. Chem. Hoppe-Seyler 382*, 1315−1320.
7. Jürgens, C., Strom, A., Wegener, D., Hettwer, S., Wilmanns, M., and Sterner, R. (2000) Directed evolution of a $(\beta\alpha)_8$-barrel enzyme to catalyze related reactions in two different metabolic pathways, *Proc. Natl. Acad. Sci. U.S.A. 97*, 9925−9930.
8. Larralde, R., Robertson, M. P., and Miller, S. L. (1995) Rates of Decomposition of Ribose and Other Sugars: Implications for Chemical Evolution, *Proc. Natl. Acad. Sci. U.S.A. 92*, 8158−8160.
9. Rudolph, J., and Stubbe, J. (1995) Investigation of the mechanism of phosphoribosylamine transfer from glutamine phosphoribosylpyrophosphate amidotransferase to glycinamide ribonucleotide synthetase, *Biochemistry 34*, 2241−2250.
10. Davisson, V. J., Deras, I. L., Hamilton, S. E., and Moore, L. L. (1994) A plasmid-based approach for the synthesis of a histidine biosynthetic intermediate, *J. Org. Chem. 59*, 137−143.
11. Sterner, R., Kleemann, G. R., Szadkowski, H., Lustig, A., Hennig, M., and Kirschner, K. (1996) Phosphoribosyl anthranilate isomerase from *Thermotoga maritima* is an extremly stable and active homodimer, *Protein Sci. 5*, 2000−2008.
12. Huang, X., Holden, H. M., and Raushel, F. M. (2001) Channeling of substrates and intermediates in enzyme-catalyzed reactions, *Annu. Rev. Biochem. 70*, 149−180.
13. Beismann-Driemeyer, S., and Sterner, R. (2001) Imidazole glycerol phosphate synthase from *Thermotoga maritima*. Quaternary structure, steady-state kinetics, and reaction mechanism of the bienzyme complex, *J. Biol. Chem. 276*, 20387−20393.
14. Margolis, M. N., and Goldberger, R. F. (1966) Isolation of the fourth (isomerase) of histidine biosynthesis from *Salmonella typhimurium*, *J. Biol. Chem. 241*, 3262−3269.
15. Sakar, G., and Sommer, S. S. (1990) The "megaprimer" method of site directed mutagenesis, *Biotechniques 8*, 404−407.
16. Barik, S. (1998) Mutagenesis by Megaprimer PCR, in *Genetic Engineering with PCR* (Horton, R. M., and Tait, R. C., Eds.) Vol. 5, pp 25−38, Horizon Scientific Press, Norfolk, U.K.
17. Thoma, R., Obmolova, G., Lang, D. A., Schwander, M., Jenö, P., Sterner, R., and Wilmanns, M. (1999) Efficient expression, purification and crystallization of two hyperthermostable enzymes of histidine biosynthesis, *FEBS Lett. 454*, 1−6.
18. Thoma, R., Hennig, M., Sterner, R., and Kirschner, K. (2000) Structure and function of mutationally generated monomers of dimeric phosphoribosylanthranilate isomerase from *Thermotoga maritima*, *Structure 8*, 265−276.
19. Merz, A., Yee, M. C., Szadkowski, H., Pappenberger, G., Crameri, A., Stemmer, W. P., Yanofsky, C., and Kirschner, K. (2000) Improving the catalytic activity of a thermophilic enzyme at low temperatures, *Biochemistry 39*, 880−889.
20. Matney, T. S., Goldschmidt, E. P., Erwin, N. S., and Scroggs, R. S. (1964) A preliminary map of genomic sites for F-attachment in *Escherichia coli* K12, *Biochem. Biophys. Res. Commun. 17*, 278−281.
21. Vogel, H. J., and Bonner, D. M. (1956) Acetylornithinase of *E. coli*: partial purification and some properties, *J. Biol. Chem. 218*, 97−106.
22. SERC (1994) The CCP4 Suite: Programs for Protein Crystallography, *Acta Crystallogr. D50*, 760−763.
23. Hennig, M., Sterner, R., Kirschner, K., and Jansonius, J. N. (1997) Crystal structure at 2.0 Å resolution of phosphoribosyl anthranilate isomerase from the hyperthermophile *Thermotoga maritima*: Possible determinants of protein stability, *Biochemistry 36*, 6009−6016.
24. Brünger, A. T. (1992) *X-PLOR Version 3.1. A System for X-ray Crystallography and NMR*, Yale University Press, New Haven, CT.
25. Jones, T. A., Zou, J. Y., Cowan, S. W., and Kjeldgaard, M. (1991) Improved methods for building protein models in electron density maps and the location of errors in these models, *Acta Crystallogr. A47*, 110−119.
26. Read, R. J. (1986) Improved Fourier coefficients for maps using phases from partial structures with errors, *Acta Crystallogr. A42*, 140−149.
27. Laemmli, U. K. (1970) Cleavage of structural proteins during the assembly of the head of bacteriophage T4, *Nature 227*, 680−685.
28. Bradford, M. M. (1976) A rapid and sensitive method for the quantitation of microgram quantities of protein utilizing the principle of protein-dye binding, *Anal. Biochem. 72*, 248−254.
29. Levine, R. L., and Federici, M. M. (1982) Quantitation of aromatic residues in proteins: model compounds for second-derivative spectroscopy, *Biochemistry 21*, 2600−2606.
30. Pace, C. N., Vajdos, F., Fee, L., Grimsley, G., and Gray, T. (1995) How to measure and predict the molar absorption coefficient of a protein, *Protein Sci. 4*, 2411−2423.
31. Stoll, V. S., and Blanchard, J. S. (1990) Buffers: Principles and Practice, *Methods Enzymol. 182*, 24−38.
32. Eberhard, M. (1990) A set of programs for analysis of kinetic and equilibrium data, *Comput. Appl. Biosci. 6*, 213−221.
33. Hommel, U., Eberhard, M., and Kirschner, K. (1995) Phosphoribosyl anthranilate isomerase catalyzes a reversible Amadori reaction, *Biochemistry 34*, 5429−5439.
34. Eisenthal, R., and Cornish-Bowden, A. (1974) The direct linear plot. A new graphical procedure for estimating enzyme kinetic parameters, *Biochem. J. 139*, 715−720.
35. Bisswanger, H., Kirschner, K., Cohn, W., Hager, V., and Hansson E. (1979) *N*-(5-Phosphoribosyl)anthranilate isomerase-indoleglycerol-phosphate synthase. 1. A substrate analog binds to two different binding sites on the bifunctional enzyme from *Escherichia coli*, *Biochemistry 18*, 5946−5953.
36. Dabrowski, S., and Kur, J. (1998) Cloning and expression in *Escherichia coli* of the recombinant his-tagged DNA polymerases from *Pyrococcus furiosus* and *Pyrococcus woesei*, *Protein Expression Purif. 14*, 131−138.
37. Rosenthal, J. A., Levandoski, M. M., Chang, B., Potts, J. F., Shi, Q. L., and Hawrot, E. (1999) The functional role of positively charged amino acid side chains in α-bungarotoxin revealed by site-directed mutagenesis of a His-tagged recombinant α-bungarotoxin, *Biochemistry 38*, 7847−7855.
38. Jaenicke, R. (1991) Protein stability and molecular adaptation to extreme conditions, *Eur. J. Biochem. 202*, 715−728.
39. Závodszky, P., Kardos, J., Svingor, A., and Petsko, G. A. (1998) Adjustment of conformational flexibility is a key event in the thermal adaptation of proteins, *Proc. Natl. Acad. Sci. U.S.A. 95*, 7406−7411.
40. Creighton, T. E., and Yanofsky, C. (1966) Indole-3-glycerol phosphate synthetase of *Escherichia coli*, an enzyme of the tryptophan operon, *J. Biol. Chem. 241*, 4616−4624.
41. Giver, L., Gershenson, A., Freskgard, P. O., and Arnold, F. H. (1998) Directed evolution of a thermostable esterase, *Proc. Natl. Acad. Sci. U.S.A. 95*, 12809−12813.
42. Van den Burgh, B., Vriend, G., Veltman, O. R., Venema, G., and Eijsink, V. G. H. (1998) Engineering an enzyme to resist boiling, *Proc. Natl. Acad. Sci. U.S.A. 95*, 2056−2060.
43. Miyazaki, K., Wintrode, P. L., Gryling, R. A., Rubingh, D. N., and Arnold, F. H. (2000) Directed evolution study of temperature adaptation in a psychrophilic enzyme, *J. Mol. Biol. 297*, 1015−1026.

44. Sterner, R., and Liebl, W. (2001) Thermophilic adaptation of proteins, *Crit. Rev. Biochem. Mol. Biol. 36*, 39−106.
45. Lang, D., Thoma, R., Henn-Sax, M., Sterner, R., and Wilmanns, M. (2000) Structural Evidence for Evolution of the β/α Barrel Scaffold by Gene Duplication and Fusion, *Science 289*, 1546−1550.
46. Hennig, M., Darimont, B., Jansonius, J. N., and Kirschner, K. (2002) The Catalytic Mechanism of Indole-3-Glycerol Phosphate Synthase: Crystal Structures of Complexes of the Enzyme from *Sulfolobus solfataricus* with the Substrate Analogue, Substrate, and Product, *J. Mol. Biol. 319*, 757−766.
47. Isabell, H. S., and Frush, H. L. (1958) Mutarotation, hydrolysis and rearrangement reactions of glycosylamines, *J. Org. Chem. 23*, 1909−1919.
48. Creighton, T. E. (1970) *N*-(5′-Phosphoribosyl)anthranilate isomerase-indol-3-glycerol phosphate synthetase of tryptophan biosynthesis. Relationship between the two activities of the enzyme from *Escherichia coli*, *Biochem. J. 120*, 699−707.
49. Kirschner, K., Szadkowski, H., Jardetzky, T. S., and Hager, V. (1987) Phosphoribosylanthranilate isomerase-indoleglycerol-phosphate synthase from *Escherichia coli*, *Methods Enzymol. 142*, 386−397.
50. Schendel, F. J., Cheng, Y. S., Otvos, J. D., Wehrli, S., and Stubbe, J. (1988) Characterization and chemical properties of phosphoribosylamine, an unstable intermediate in the de novo purine biosynthetic pathway, *Biochemistry 27*, 2614−2623.
51. Eder, J. (1991) Folding, stability and catalytic mechanism of an eightfold β/α-barrel protein studied by protein engineering, Ph.D. Thesis, University of Basel, Basel, Switzerland.
52. Jaenicke, R. (2000) Do ultrastable proteins from hyperthermophiles have high or low conformational rigidity? *Proc. Natl. Acad. Sci. U.S.A. 97*, 2962−2964.
53. Gerber, P. R. (1992) Peptide mechanics: a force field for peptides and proteins working with entire residues as smallest units, *Biopolymers 32*, 1003−1017.

BI026092H